Geophys. J. Int. (2009) **177,** 33–42 doi: 10.1111/j.1365-246X.2009.04043.x

Magnetite magnetosome and fragmental chain formation of *Magnetospirillum magneticum* AMB-1: transmission electron microscopy and magnetic observations

Jinhua Li,[1] Yongxin Pan,[1] Guanjun Chen,[2] Qingsong Liu,[1] Lanxiang Tian[1] and Wei Lin[1]

[1]*Biogeomagnetism Group, Paleomagnetism and Geochronology Laboratory (SKL-LE), Institute of Geology and Geophysics, Chinese Academy of Sciences, Beijing* 100029, *China. E-mail: yxpan@mail.iggcas.ac.cn*
[2]*State Key Laboratory of Microbial Technology, School of Life Science, Shandong University, Jinan* 250100, *China*

Accepted 2008 November 25. Received 2008 November 25; in original form 2008 July 2

SUMMARY

Stable single-domain (SD) magnetite formed intracellularly by magnetotactic bacteria is of fundamental interest in sedimentary and environmental magnetism. In this study, we studied the time course of magnetosome growth and magnetosome chain formation (0–96 hr) in *Magnetospirillum magneticum* AMB-1 by transmission electron microscopy (TEM) observation and rock magnetism. The initial non-magnetic cells were microaerobically batch cultured at 26 °C in a modified magnetic spirillum growth medium. TEM observations indicated that between 20 and 24 hr magnetosome crystals began to mineralize simultaneously at multiple sites within the cell body, followed by a phase of rapid growth lasting up to 48 hr cultivation. The synthesized magnetosomes were found to be assembled into 3–5 subchains, which were linearly aligned along the long axis of the cell, supporting the idea that magnetosome vesicles were linearly anchored to the inner membrane of cell. By 96 hr cultivation, 14 cubo-octahedral magnetosome crystals in average with a mean grain size of ∼44.5 nm were formed in a cell. Low-temperature (10–300 K) thermal demagnetization, room-temperature hysteresis loops and first-order reversal curves (FORCs) were conducted on whole cell samples. Both coercivity (4.7–18.1 mT) and Verwey transition temperature (100–106 K) increase with increasing cultivation time length, which can be explained by increasing grain size and decreasing non-stoichiometry of magnetite, respectively. Shapes of hysteresis loops and FORCs indicated each subchain behaving as an 'ideal' uniaxial SD particle and extremely weak magnetostatic interaction fields between subchains. Low-temperature thermal demagnetization of remanence demonstrated that the Moskowitz test is valid for such linear subchain configurations (e.g. $\delta_{FC}/\delta_{ZFC} > 2.0$), implying that the test is applicable to ancient sediments where magnetosome chains might have been broken up into short chains due to disintegration of the organic scaffold structures after cell death. These findings provide new insights into magnetosome biomineralization of magnetotactic bacteria and contribute to better understanding the magnetism of magnetofossils in natural environments.

Key words: Biogenic magnetic minerals; Environmental magnetism; Rock and mineral magnetism.

1 INTRODUCTION

Magnetotactic bacteria (MTB) have the capability of producing tailored magnetosomes, which are single-domain (SD) magnetic crystals consisting of magnetite (Fe_3O_4) or greigite (Fe_3S_4) particles each enveloped by a lipid bilayer membrane (Bazylinski & Frankel 2004; Komeili *et al.* 2004). Because of their unique crystalline, magnetic and biochemical characteristics, unraveling the formation mechanism of magnetosomes and identifying the fossil magnetosomes (also named magnetofossils) are of fundamental interest in geosciences, biomineralization and biology (Bazylinski & Frankel 2004; Pan *et al.* 2005a; Pósfai *et al.* 2006a; Komeili 2007; Kopp & Kirschvink 2008).

Magnetofossils have been found in a variety of depositional environments, from present to Mesozoic, and possibly of Precambrian age (Chang *et al.* 1989; Pan *et al.* 2005a; Housen & Moskowitz 2006; Lippert & Zachos 2007; Maloof *et al.* 2007; Kopp & Kirschvink 2008). Because MTB prefer to live within the oxic/anoxic interface (OAI), which is generally located at sediment–water interface or within a chemically stratified water column,

magnetofossils can convey very useful information about palaeoecology and palaeoclimate (Hesse 1994; Snowball *et al.* 2002; Paasche *et al.* 2004; Linford *et al.* 2005). In addition, SD magnetofossils contribute significantly to the magnetic signature of aquatic sediments and soils (Egli 2004; Kim *et al.* 2005; Pan *et al.* 2005a; Housen & Moskowitz 2006). The cultivatable MTB strains provide unique opportunities to study magnetosome and chain formation under controlled laboratory conditions and their associated rock magnetic properties.

The most significant structural feature of MTB is that their magnetosomes are usually arranged in the form of a single or multiple chains, which serve as an intracellular biocompass and facilitate orientation along the geomagnetic field lines (Frankel *et al.* 1997). Recent molecular biology and cryo-electron tomography studies suggested that magnetosome chain is fixed inside the cell body by an organic scaffold, that is, a cytoskeletal structure and anchoring proteins (Kobayashi *et al.* 2006; Komeili *et al.* 2006; Scheffel *et al.* 2006). Nevertheless, the dynamics of chain formation in MTB is not well understood and needs to be examined experimentally. Here, we provide important constrains on the dynamics of magnetosome chain formation.

To detect magnetofossils in natural sediment sample, Moskowitz *et al*. (1993) proposed a rockmagnetic test uniquely sensitive to the presence of magnetite crystals arranged in chains. A positive test is obtained when the δ ratio (δ_{FC}/δ_{ZFC}) is greater than 2.0. The δ ratio reflects the difference of remanence losses passing the Verwey transition between the field-cooled (FC) and zero-field cooled (ZFC), where $\delta = (M_{80K} - M_{150K})/M_{80K}$, and M_{80K} and M_{150K} are the remanences measured at 80 and 150 K, respectively, that is, well below and above the temperature T_v of the Verwey transition in magnetite. The Moskowitz test relies on two factors: higher magnetocrystalline anisotropy of magnetite in the monoclinic phase ($T < T_v$) than in the cubic phase ($T > T_v$) and second, shape anisotropy produced by the chain arrangement. It has been demonstrated that the test is valid for both cultured and uncultured MTB cell samples where cells contain complete chains of magnetosomes (Moskowitz *et al.* 1993, 2008; Pan *et al.* 2005b). However, failures of the Moskowitz test (i.e. δ ratios less than 2.0) were also reported due to smearing, or even, of the absence of the Verwey transition as a result of magnetosome oxidation (i.e. non-stoichiometry) or due to the presence of superparamagnetic (SP) magnetite particles (Moskowitz *et al.* 1993; Weiss *et al.* 2004; Fischer *et al.* 2008).

Moreover, besides forming a complete magnetosome chain, *Magnetospirillum magneticum* AMB-1 (hereafter referred to AMB-1) can also form fragmental chains separated by gaps (Kopp *et al.* 2006), depending on the growth conditions. These unconventional fragmental chains could provide new insights into not only the mechanism of magnetosome biomineralization but also the magnetic properties. For instance, it is not clear whether the Moskowitz test is still valid for the fragmental chains, which could be common for magnetofossils in sediments and sedimentary rocks.

In this study, we aim to demonstrate that fragmental chains can be consistently formed by AMB-1 in controlled laboratory conditions and further to monitor how they develop with cultivation time (0–96 hr). The temporal changes of magnetosome growth and magnetic properties throughout the cell growth phases were carefully studied by a combination of transmission electron microscopy (TEM) and rock magnetic methods [low-temperature magnetic measurements, room-temperature hysteresis loops and first-order reversal curves (FORCs)]. Finally, we discussed the biophysical and geological significance of our findings.

2 MATERIALS AND EXPERIMENTAL METHODS

2.1 Strain, culture condition and sampling

The AMB-1 strains used in this study were purchased from the American Type Culture Collection (ATCC700264; Matsunaga *et al.* 1991). They were cultured in a modified magnetic spirillum growth medium (MSGM; Yang *et al.* 2001). The time-course growth experiment started from non-magnetic AMB-1 cells (without any intracellular magnetosomes; Fig. 1a), which were obtained through a 36-hr aerobic incubation of AMB-1 strains. About 2-mL non-magnetic cell suspension was inoculated into each of the 96 serum vials that contained 250-mL MSGM with about 50-mL headspace. The vial was sealed with a butyl-rubber stopper after the inoculation to avoid further gas exchange with ambient air. During the whole experiment, all vials were treated statically and cells were microaerobically cultured at 26 °C. For the detailed description of the used chemical composition of growth medium, non-magnetic cells preparation and inoculation procedures, see the Appendix.

Cells were collected at 0, 10, 20, 24, 28, 32, 36, 40, 44, 48, 52, 56, 60, 68, 76 and 96 hr (total 16 steps) to monitor cell growth, magnetosome and chain formation. At each given time, cell samples were enriched from six fresh (not sampled) vials. Magnetic experiments were performed on whole cell samples cultivated at 28, 36, 48, 68 and 96 hr of different growth phases (see Section 3.1 and Table 1). For magnetic measurements, fresh cells were harvested by centrifuging the cell suspensions at 10 000 rpm for 15 min at 4 °C using an Eppendorf 5804(R) centrifuge.

2.2 OD_{600} and TEM analyses

Cell growth at a given time was monitored by measuring the optical density of cell suspensions at 600 nm (OD_{600}), using a spectrophotometer (Model 722 spectrophotometer, Shanghai Hanson Instrument).

TEM analyses were performed on a JEM-100CXII TEM at an accelerating voltage of 80 kV. The magnetosome numbers were counted from at least 50 cells (up to 221 cells). The crystal sizes were determined by measuring the major (length, L) and minor (width, W) axes of the best-fitting ellipse of the 2-D bright-field TEM images. The grain size was defined as $(L + W)/2$, and the shape factor as W/L.

To evaluate the spatial distribution of magnetosomes and subchain (see Section 3.1), centre-to-centre distance between two adjacent magnetosomes within a subchain (d_{cc}) and inter-subchain distance (d_{sc}; defined as the nearest centre-to-centre distance between two end crystals in adjacent subchains) were analysed by counting at least 100 particles.

2.3 Low-temperature magnetic measurements

Low-temperature magnetic experiments were performed on the whole cell samples using a Quantum Design Magnetic Property Measurement System (MPMS XP-5, sensitivity is 5.0×10^{-10} A m^2). Saturation remanence acquired in a 5-T field at 10 K (hereafter termed $SIRM_{5T-10K}$) was demagnetized and measured by warming from 10 to 300 K following two different magnetic field pre-treatments. The first was produced by cooling the cell samples down from 300 to 10 K in a zero magnetic field (ZFC), whereas the second was produced by cooling the cell samples from

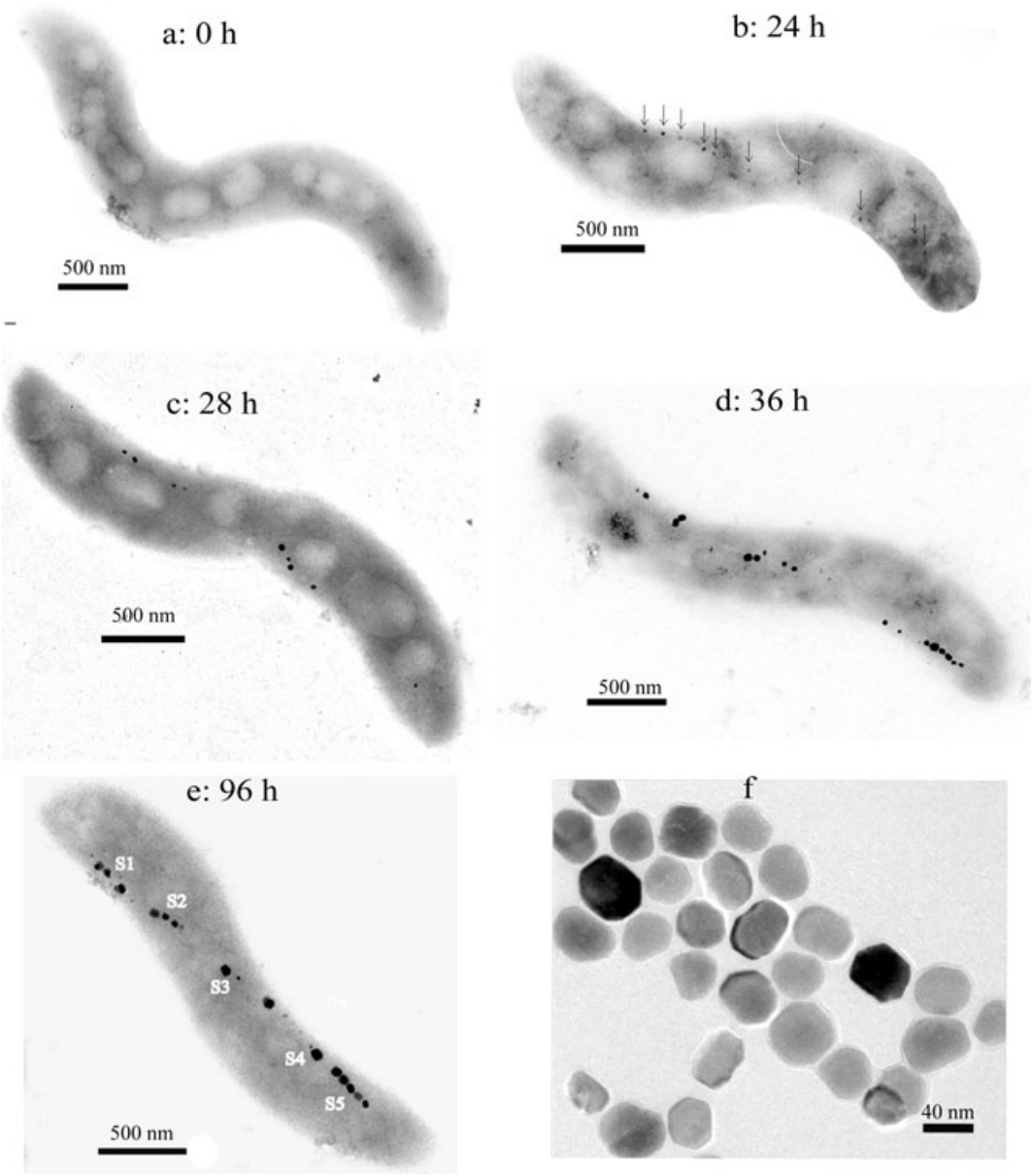

Figure 1. Representative transmission electron microscopy (TEM) images of whole AMB-1 cells cultivated at different times. (a) Initial non-magnetic cell; (b) 24-hr cultivated cell with fine-grained magnetosomes (marked by arrows); (c) 28-hr cultivated cell; (d) 36-hr cultivated cell; (e) 96-hr cultivated cell showing magnetosome subchains (marked by Sn); (f) extracted magnetosomes from cells at 96-hr cultivation.

300 to 10 K in a 5-T field (FC). The Verwey transition temperature (T_v) is defined as the temperature for the maximum of the first-order derivative of dM/dT from the FC curve. The δ ratio (δ_{FC}/δ_{ZFC}) was calculated after Moskowitz *et al*. (1993).

2.4 Room-temperature hysteresis loops and FORCs

Room-temperature hysteresis loops and FORCs were measured using an Alternating Gradient Force Magnetometer Model Micro-Mag 2900 (Princeton Measurements Corporation, sensitivity is 1.0×10^{-11} A m^2). The hysteresis loops were measured between $\pm$1.5 T with an averaging time of 100 ms. Saturation magnetization (M_s), saturation remanence (M_{rs}) and coercivity (B_c) were determined after correction for linear contributions from the diamagnetic and paramagnetic phases. Subsequently, the SIRM acquired at 1.5 T was demagnetized in a backfield to obtain the coercivity of remanence (B_{cr}). Each FORC was measured by saturating the cell sample at 1.2 T, decreasing the field to a value of H_a, and reversing the field sweep to the saturated state in a series of steps following the protocol described in Roberts *et al*. (2000). FORC diagrams were calculated using the FORCO-BELLO MATLAB code version 0.99c with a smoothing factor (SF) of 3 (Winklhofer & Zimanyi 2006). In a FORC diagram, the horizontal and vertical axes usually are referred to as microcoercivity (H_c) and interaction field, respectively. Strictly speaking, this assignment is only true for a system in which each particle is characterized by a rectangular hysteresis loop (Winklhofer & Zimanyi 2006). At the other extreme, in a non-interacting assemblage of randomly oriented Stoner–Wohlfarth type particles, the vertical axis cannot have the meaning of an interaction field, and should rather be referred to as bias field (H_b), which

Table 1. Data of cell growth, magnetosome and subchain formation of AMB-1 at different growth stages.

Growth phase	Time (hr)	Cells	Magnetosomes				Magnetosome chains		
		OD_{600}	N_m	L_m (nm)	W_m (nm)	Shape factor	Subchain number	d_{sc} (nm)	d_{cc} (nm)
	0	0.000	0	–	–	–	–	–	–
Lag phase	10	0.000	0	–	–	–	–	–	–
	20	0.008	0	–	–	–	–	–	–
	24	0.017	6 ± 4	24.3 ± 4.5	19.1 ± 5.2	0.79	–	–	–
	28	0.018	6 ± 3	36.0 ± 11.7	30.1 ± 10.5	0.84	3 ± 1	221.3 ± 124.2	57.9 ± 10.4
	32	0.032	9 ± 4	42.8 ± 10.7	35.8 ± 10.4	0.83	4 ± 2	245.1 ± 153.7	60.5 ± 9.1
Exponential phase	36	0.036	11 ± 3	43.9 ± 12.1	36.1 ± 11.2	0.82	4 ± 1	273.6 ± 131.8	59.8 ± 9.6
	40	0.041	9 ± 3	42.9 ± 10.4	37.2 ± 10.4	0.86	4 ± 1	286.4 ± 132.1	62.5 ± 9.6
	44	0.083	12 ± 3	43.8 ± 12.4	36.8 ± 11.3	0.84	5 ± 2	243.4 ± 134.9	61.5 ± 9.6
	48	0.107	12 ± 5	44.4 ± 12.1	37.5 ± 11.3	0.84	4 ± 1	239.0 ± 127.3	61.8 ± 10.0
	52	0.107	12 ± 3	45.7 ± 10.7	39.9 ± 10.1	0.87	4 ± 1	290.0 ± 158.6	61.9 ± 10.3
	56	0.105	11 ± 3	44.2 ± 12.3	37.2 ± 11.5	0.84	4 ± 2	283.1 ± 162.3	60.6 ± 9.4
Stationary phase	60	0.098	12 ± 4	47.2 ± 12.5	39.6 ± 11.6	0.84	4 ± 1	283.1 ± 198.6	57.9 ± 11.7
	68	0.095	13 ± 4	46.1 ± 13.1	38.4 ± 11.7	0.83	5 ± 1	273.6 ± 185.6	55.9 ± 12.1
	76	0.081	14 ± 3	45.5 ± 13.1	39.2 ± 12.6	0.86	4 ± 2	276.7 ± 157.5	58.6 ± 9.6
	96	0.082	14 ± 3	48.2 ± 13.8	40.8 ± 12.9	0.85	4 ± 1	247.0 ± 125.5	56.9 ± 10.3

Note: OD_{600} refers optical density of cell suspensions; N_m indicates the averaged magnetosome number per cell; L_m and W_m indicate the mean grain length and width of magnetosome, respectively; d_{sc} indicates the inter-subchain distance within cells, d_{cc} indicates the centre-to-centre distance between adjacent magnetosomes within subchains.

reflects the history-dependence of magnetization changes (Newell 2005). Also, for non-interacting particles, the contributions to the FORC diagram for negative values of H_b do not reflect irreversible switching events, but history-dependent reversible magnetization changes, as shown theoretically by Newell (2005) and experimentally by Winklhofer *et al.* (2008).

3 RESULTS

3.1 Cell and magnetosome growth, and magnetosome subchain

Based on the OD_{600} data, the time-course cell growth can be divided into three phases (Table 1). The cell numbers increase very slowly during a lag phase (0–20 hr), increase rapidly during an exponential phase (20–48 hr) and decrease slowly during a stationary phase (48–96 hr). The death phase, which is characteristic of exponential decrease in cell numbers, did not occur until 96 hr in this study.

The number and the grain size of magnetosomes and chain arrangements are summarized in Table 1. No magnetosomes were visually observed in the AMB-1 cells during the lag phase. At 24 hr, about 10 per cent of cells produced very fine-grained magnetosomes which were detected at multiple positions within the cell body (Fig. 1b, arrows). After 32 hr cultivation and later, almost all cells formed magnetosomes; magnetosomes in a bacterium were arranged in the form of several short chains along the long axis of the cell (see Figs 1c–e).

Under the used growth conditions, the vast majority of cells (>90 per cent) formed fragmental chains. The fragmental chain commonly consists of 3–5 short chains with large gaps (hereafter referred to as subchains). Each subchain contains 3–6 closely aligned magnetosomes. Smaller magnetosomes are usually formed at the end of a subchain. Nevertheless, the subchains were linearly aligned along the long axis of the cell. The centre-to-centre distance d_{cc} varies from 55.9 to 62.5 nm and is nearly constant during the whole time course (Table 1). The distance between adjacent subchains d_{sc} varies from ∼221 to ∼290 nm (Table 1). These snapshots at different stages of cell growth suggest that the relative position of a magnetosome within a subchain is likely fixed.

To quantify the magnetosome growth, the averaged magnetosome number per cell (N_m), length (L_m) and width (W_m) of magnetosome, and shape factor were analysed (see Table 1). Statistically, the N_m, L_m and W_m increase rapidly during the early exponential phase. Between 32 and 48 hr, the cells divide faster, while the N_m still increases, indicating that magnetosomes were synthesized fast enough to compensate for the accelerated cell division. The slight decrease of N_m at 40 hr suggests that magnetosome formation lags behind cell division at the end of the exponential phase. During the stationary phase, the cell number decreases with time, but the N_m and grain sizes still increase slightly. After 96 hr cultivation, in average, the cell produced 14 cubo-octahedral magnetosome crystals with a mean grain size of 44.5 nm (Figs 1e and f).

Fig. 2 shows the grain size and shape factor distributions of magnetosomes at 28 , 32 and 68 hr. The grain size distribution evolves gradually from positively skewed (skewness of 0.17 at 28 hr) to negatively skewed shape (skewness of −0.29 at 32 hr and −0.52 at 68 hr). The positively skewed shape of the crystal size distribution represents the unconstrained growth (i.e. not limited by vesicles size). With the magnetosome growing, the spatial limitation of vesicles possibly results in forming a negatively skewed distribution. The shape factor distributions of magnetosomes throughout the cell cultivation were very narrow and asymmetric, also indicating a strictly biochemical control on magnetosome formation (Eberl *et al.* 1998; Arató *et al.* 2005).

3.2 The Verwey transition and the Moskowitz test

Fig. 3 shows representative low-temperature magnetization curves and room-temperature hysteresis loops of the cell samples. Both FC and ZFC warming curves show a sharp drop of $SIRM_{5T-10K}$ intensity around 100–106 K (Figs 3a, c and e), indicative of magnetite magnetosomes. Specifically, the T_v is of 100, 104, 104, 104 and 106 K for the cell samples at 28, 36, 48, 68 and 96 hr, respectively. On the warming curves after FC, those samples showed about 90.9, 58.6, 49.8, 44.2 and 51.7 per cent of $SIRM_{5T-10K}$ loss at 300 K,

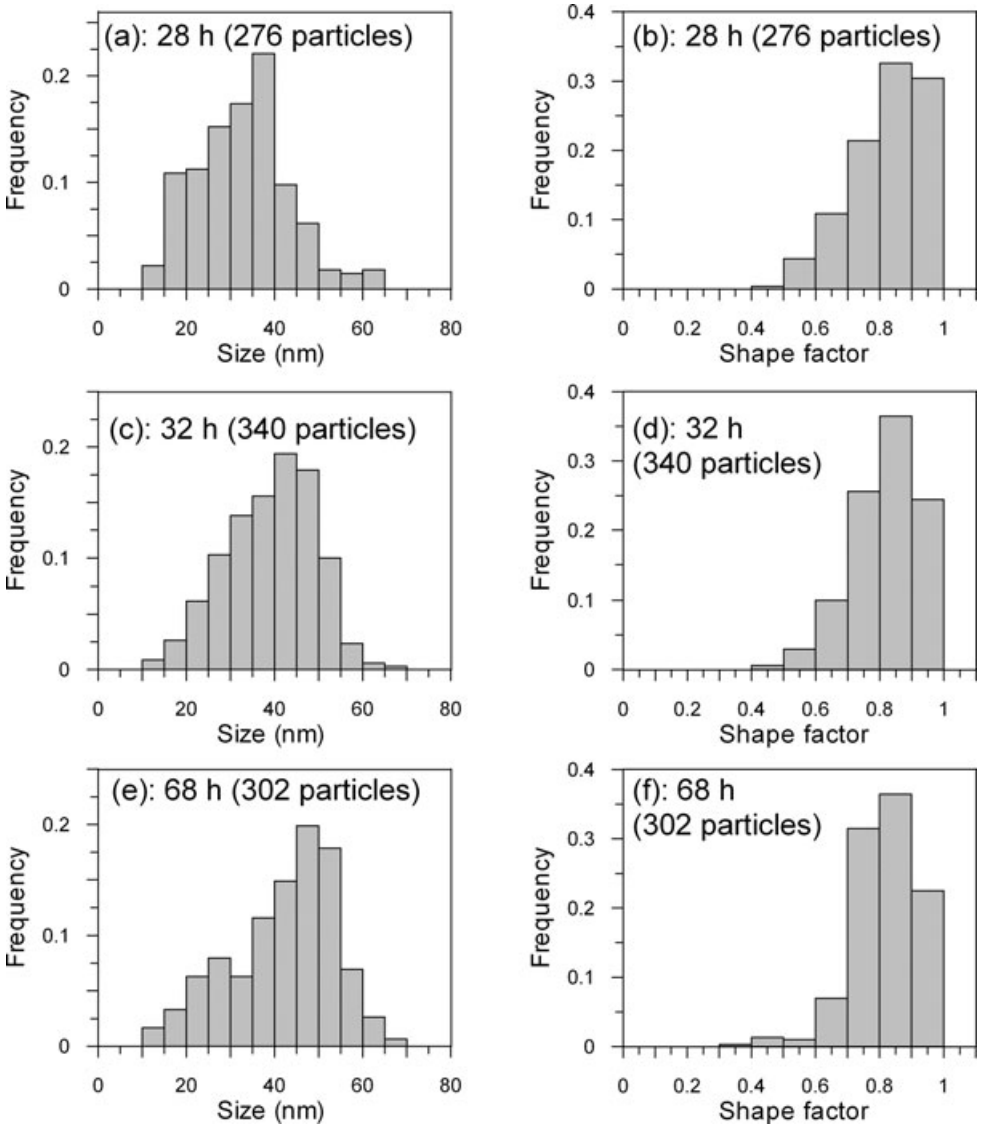

Figure 2. Crystal size distributions (left-hand side) and shape factor distributions (right-hand side) of magnetosomes at 28, 32, and 68 hr. Size equals $(W + L)/2$.

respectively. The decreasing demagnetization through warming and increasing T_v with cultivation time suggest a decreasing contribution of SP particles and an evolution towards more stoichiometric magnetite (Aragón *et al.* 1993; Muxworthy & McClelland 2000). The observed remanence losses at 300 K by low-temperature demagnetization are much bigger than those of other cultured and uncultured MTB (see table 2 in Pan *et al*. 2005b). It is likely due to the smaller grain size formed and much shorter chains in this study. However, the T_v values (100–106 K) are comparable to other values published (see Pan *et al*. 2005b), suggesting that grain size effect on the T_v value is limited (Prozorov *et al.* 2007).

The calculated δ_{FC}/δ_{ZFC} values increase from 1.3 at 28 hr to $\geq$2.0 after 36 hr. For the cell samples at 36, 48, 68 and 96 hr, their δ ratios are 2.2, 2.1, 2.3 and 2.0, respectively.

3.3 Hysteresis loops and FORCs

The room-temperature hysteresis loop for the cell sample at 28 hr is slightly wasp-waisted with the lowest B_c, B_{cr} and M_{rs}/M_s, but the highest B_{cr}/B_c, falling into the region with higher SP content (Fig. 3b). This is well consistent with the TEM observation and low-temperature magnetic measurement, which indicate a mixture of SP and SD particles. Other cell samples cultivated for longer time showed nearly classic Stoner–Wohlfarth type hysteresis loops with increasing coercivity values (Figs 3d and f). On the modified Day plot, the cell sample at 28 hr falls within the SD + SP region, while the other cell samples are located well in the SD grain size region (Fig. 4). The M_{rs}/M_s values are close to 0.5, which indicates that the magnetization within the cells is dominated by uniaxial anisotropy (imparted by the magnetosome chain or subchain structure, which outweighs the intrinsic cubic magnetocrystalline anisotropy; Stoner & Wohlfarth 1948). The B_c increases from 4.7 mT at 28 hr to 18.1 mT at 96 hr; and the B_{cr} increases from 11.2 mT at 28 hr to 23.3 mT at 96 hr.

FORC diagrams may provide detailed information about the distributions of coercivity and magnetostatic interaction fields, and the domain state of magnetic components (Pike *et al.* 1999; Roberts *et al.* 2000). FORC diagrams for the representative whole cell samples are shown in Fig. 5. Consistent with TEM observations, the

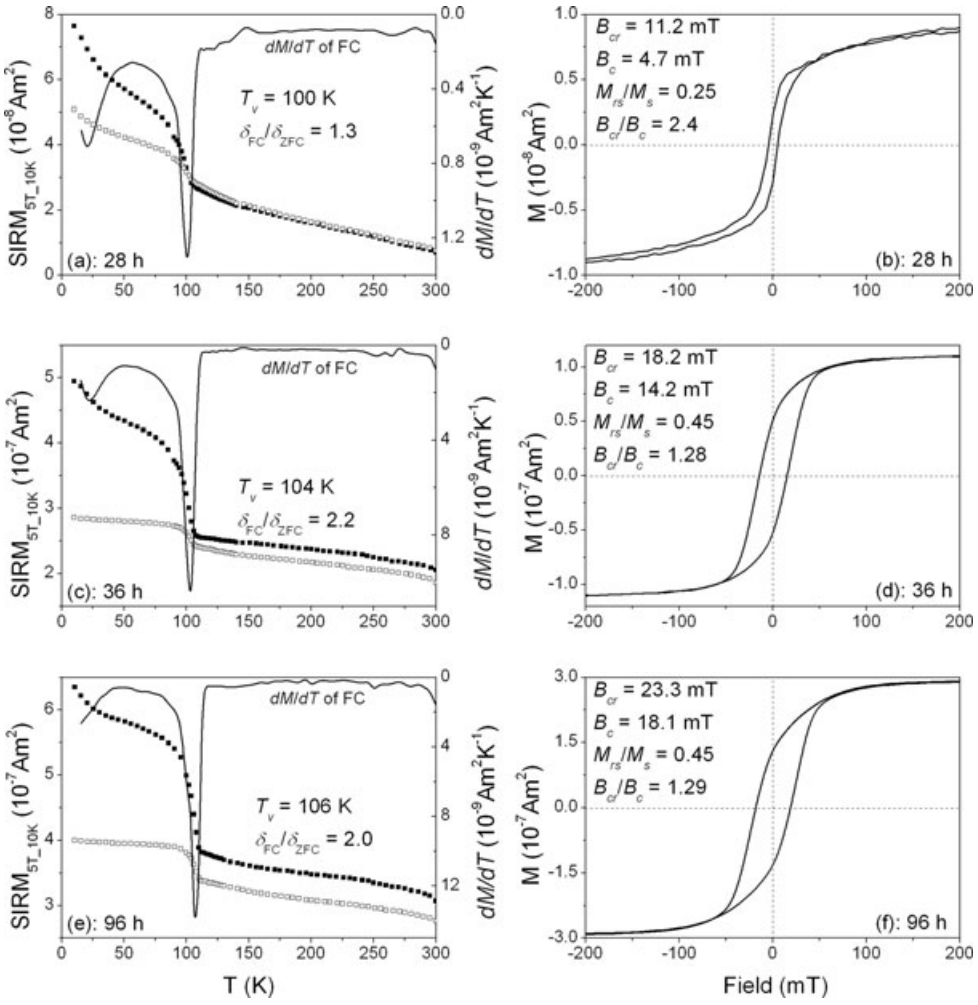

Figure 3. Low-temperature magnetic measurements and room-temperature hysteresis loops for the cell sample at 28, 36 and 96 hr. Solid (open) squares indicate the FC (ZFC) data. Thin line stands for the dM/dT of FC data, its peak reflects the $T_{\rm v}$. The calculation of $\delta_{\rm FC}/\delta_{\rm ZFC}$ ratio sees the text.

FORC diagrams for the whole AMB-1 cells show a very clear evolution from a mainly SP pattern to an SD pattern. Specifically, as expected for very small grain size and less magnetosomes, the FORC diagram for the 28 hr sample is 'noise' (Fig. 5a). The FORC distribution of cell sample at 36 hr already indicates the presence of stable SD particles with a small fraction of viscous SD (close to $H_c = 0$; Fig. 5b). Obviously, the viscous SD fraction is too small to influence the shape of the hysteresis loop, which is not constricted (Fig. 3d). And finally, the FORC diagram for the cell sample at 96 hr shows a typical SD behaviour (Fig. 5c).

The FORC diagrams for the whole AMB-1 cells after 36 hr cultivation show rather narrow vertical distribution along the H_c axis (Figs 5b and c), very different from the ones obtained for interacting magnetite particles (Muxworthy *et al.* 2004; Pan *et al.* 2005b). The latter shows a large vertical spread, while the FORC diagrams obtained here are confined to within a few mT of either side of the H_c axis. The little vertical spread appears to be due to processing-related smoothing, as the diagrams become increasingly concentrated along the H_c axis for decreasing values of SF. Interestingly, the FORC diagram in Fig. 5(c) has a pronounced negative region in the lower-left domain, centred about the point $(H_c, H_b) = (0, -30)$ mT, which is connected to the maximum of the distribution at $(H_c, H_b) = (-30, 0)$ mT by a line with slope 45°. That is exactly what Newell predicted for a non-interacting, isotropically oriented Stoner–Wohlfarth assemblage (Newell 2005). This observation supports the interpretation of the corresponding major hysteresis loop (Fig. 3f) in terms of a 'Stoner–Wohlfarth' loop. From this analogy, we may conclude that magnetostatic interactions are too small to noticeably affect the magnetic hysteresis properties.

4 DISCUSSION

4.1 Magnetosome synthesis in AMB-1

In the present study, no magnetosomes were detected during the lag phase despite non-magnetic AMB-1 cells growing in iron-rich conditions. The temporal variations of average magnetosome numbers, mean grain sizes and cell numbers suggest that the AMB-1 cells synthesize magnetosomes during both the exponential and stationary growth phases, but dominantly in the former phase (Table 1). This is different from the growth of AMB-1 under anaerobic conditions, which produced magnetosomes only in the exponential growth phase (Matsunaga *et al.* 1996; Yang *et al.* 2001). Komeili *et al.* (2004) showed that non-magnetic AMB-1 cells formed full-sized magnetosomes within 21 hr after transited into iron-rich medium. This suggests that both the initial cells and the culture environments affect the magnetosome formation in AMB-1. For instance,

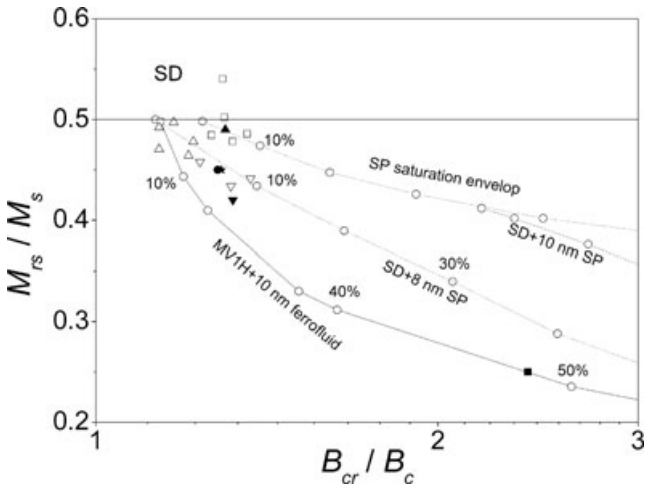

Figure 4. Measured M_{rs}/M_s and B_{cr}/B_c data for the AMB-1 cells (solid symbols, this study) compared to the other MTB (open symbols, data from (Moskowitz *et al.* 1993), the mixture of MV1H + 10 nm ferrofluid (Carter-Stiglitz *et al.* 2001) and the predictions of linear mixing theory (Dunlop 2002). Samples of the AMB-1 cells at 28 hr (square), 36 hr (circle), 48 hr (inverse triangle), 68 hr (triangle) and 96 hr (asterisk); the wet MV-1 and MV-2 (squares), freeze-dried MV-1 (triangles) and freeze-dried MS-1 (inverse triangles) cells.

Komeili *et al*. (2004) prepared their initial non-magnetic cells by pre-culturing AMB-1 strains anaerobically in iron-poor medium, and the time-course experiments were carried out under anaerobic conditions. Therefore, rapid magnetosome formation may be ubiquitous in optimal natural conditions.

The reduced T_v of magnetosome magnetite has been observed in other cultured and uncultured MTB cell samples (Moskowitz *et al.* 1993, 2008; Carter-Stiglitz *et al.* 2004; Weiss *et al.* 2004; Pan *et al.* 2005b; Kopp *et al.* 2006; Pósfai *et al.* 2006b; Prozorov *et al.* 2007). Generally speaking, cation substitution, oxidation and cation vacancies can reduce the T_v (Muxworthy & McClelland 2000; Walz 2002). Previous experiments showed that MTB formed magnetite has highly chemical purity even with titanium, chromium, cobalt, copper, nickel, mercury or lead in growth medium (Gorby 1989). Oxidation caused by sample handling in this study should be slight because fresh cells were quickly centrifuged at low temperature (4 °C) for short time (15 min) and taken for the low-temperature measurements immediately. Cation vacancies (Frankel *et al.* 1979) or crystal defects (Devouard *et al.* 1998) cannot be excluded at this stage. Although the exact mechanism for the lower T_v of magnetosomes is not determined, our data support the idea that the lower T_v may be an intrinsic property of magnetosome magnetite (Pan *et al.* 2005b; Fischer *et al.* 2008; Moskowitz *et al.* 2008).

4.2 Mechanism of subchain assemblage

Recently, Komeili (2007) proposed a new mechanism for magnetosome formation of AMB-1 involving in three steps: (1) invagination of magnetosome membrane from the inner membrane of cell; (2) integration of the membrane invaginations into a intact chain with the help of cytoskeletal filaments and (3) biomineralization of magnetite particles within the empty membrane invaginations pre-aligned within and anchored to the inner membrane of the cell. TEM observations of this study clearly showed that the magnetosome formation in AMB-1 starts simultaneously at multiple sites within cell body along the long axis of the cell. Gradually,

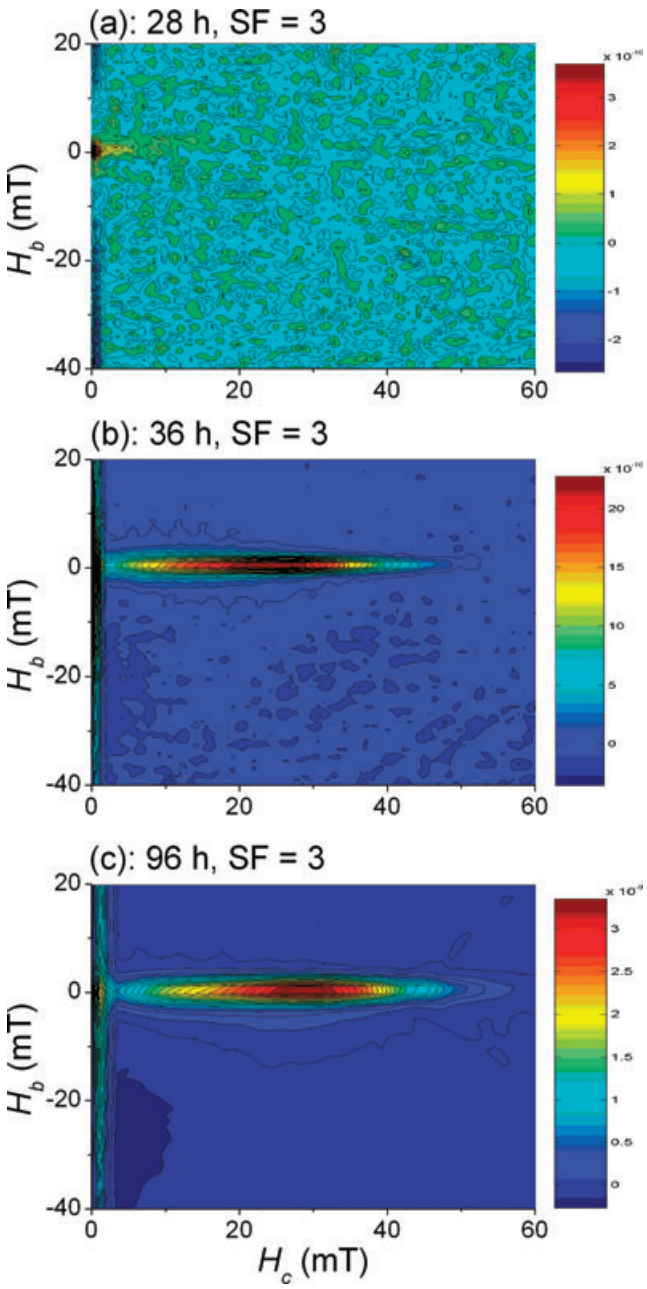

Figure 5. FORC diagrams for the AMB-1 cell sample at 28 (a), 36 (b) and 96 hr (c). A lower-left 'negative region' can be observed for the 96-hr sample.

the adjacent magnetosomes were assembled into 3–5 subchains, and the newly formed magnetosomes are added to the end of the subchains. The subchain pattern was observed till the final stage. Although the empty membrane invaginations and the cytoskeletal filaments were not detected in this study, the observations of linear arrangement of magnetosomes along the long axis of the cell and constant d_{cc} values strongly support Komeili's model. The physical connection of magnetosome vesicles to inner membrane and to cytoskeletal filaments within cell may maintain the linear arrangement of subchains. A different mechanism for the chain arrangement in *Magnetospirillum gryphiswaldense* MSR-1 was proposed, in which magnetosome biomineralization initiates simultaneously at multiple discrete sites along the entire length of the cell; and then the growing magnetosomes shift towards the mid-cell to form a straight, tightly

packed chain (Scheffel *et al.* 2006; Faivre *et al.* 2007). This different dynamics of magnetosome-chain assemblage might result from fundamental differences in the molecular mechanisms of different MTB species.

A significant observation in this study is AMB-1 formed 3–5 subchains under the used culture conditions. Several factors should be considered. Previous study revealed that no magnetosomes were formed by AMB-1 when oxygen in gas phase exceeded 35 per cent (Yang *et al.* 2001). We grew AMB-1 in microaerobic condition (∼21 per cent oxygen in the gas phase at initial time), which could inhibit magnetosome formation. Second, the used batch way culture (without subsequent iron-feeding) may lead to insufficient supply of available iron during stationary growth phase. Third, the retrogression of the initial non-magnetic cells (aerobic culture) possibly deteriorates the magnetosome formation ability of cells. To fully understand the subchain formation, further experiments (i.e. iron-feeding and various growth conditions) are needed.

4.3 Magnetostatic interaction of magnetosome subchains

The magnetostatic interactions in MTB cell samples could arise from the intrachain, interchain and intercell interactions. Previously theoretical and experimental studies have revealed that magnetostatic interactions inside magnetosome chain along the direction of the chain lead to the entire chain to behave in a magnetically coherent fashion (Penninga *et al.* 1995; Hanzlik *et al.* 2002), and to act as an 'ideal' uniaxial Stoner–Wohlfarth particle (Dunin-Borkowski *et al.* 1998; Simpson *et al.* 2005; Pósfai *et al.* 2006a). The subchain configuration of AMB-1 cells in present study provides an opportunity to study the inter-subchain and intra-subchain interactions. As clearly seen in hysteresis loops (Figs 3d and f) and FORCs (Figs 5b and c), these subchains behave as uniaxial Stoner–Wohlfarth particles. There are significant intra-subchain interactions and nearly negligible interactions between subchains. The large d_{sc} (>200 nm) and good separation of whole cells also cause weak or negligible inter-subchain and intercell interactions.

The absence of interaction characteristics also corroborate the earlier studies that FORC diagram cannot detect strong intrachain interactions of magnetosomes because each magnetosome chain acts as an individual elongated SD particle (Pan *et al.* 2005b; Chen *et al.* 2007). This idea was independently supported by magnetic induction mapping of multiple magnetosome chains in MTB using electron holography (Simpson *et al.* 2005; Pósfai *et al.* 2006a).

4.4 More geological significance

In nature, MTB commonly inhabit in OAI in aquatic environments with a high cell concentration of 10^5–10^6 cells mL^{-1}. The OAI system can provide MTB with beneficial vertical redox and chemical gradients, and relatively high concentration of dissolved iron (Simmons *et al.* 2004; Simmons & Edwards 2006; Moskowitz *et al.* 2008). Thus, the natural environments have advantages for magnetosome formation compared with laboratory culture conditions. So far, the direct observation of MTB growth in natural environment is not practically feasible. Detailed studies on the cultivated MTB strains are still crucial for understanding the mechanism of magnetosome formation and their biogeochemical significances, for example, nitrogen fixation, nitrogen denitrification and iron cycling, despite that there could be dramatic differences between the laboratory condition and natural environment. If fragmental chain were found to exist in other cultivated or uncultivated MTB, the subchain pattern and experimental conditions used in this study may provide very useful reference to account for the fragmental chain formation.

Importantly, the present study shows for the first time that the Moskowitz test is still valid for subchains of magnetosomes (Figs 1, 3c and e). The failure of Moskowitz test for the cell sample at 28 hr is obviously due to the presence of a high-fraction SP particles and very poor chain formation, as indicated by the shape of warming curve (Fig. 3a), hysteresis loop (Fig. 3b) and FORC diagram (Fig. 5a). All other four measured samples (36, 48, 68 and 96 hr) successfully passed the test. This finding significantly expands the practicality of the test to identify magnetofossils in ancient sediments. Besides, the observed lower T_v (100–106 K) for the cultivated AMB-1 suggests a reduced stoichiometry of magnetite magnetosomes.

It is realized that magnetic minerals in sediments, usually a mixture of biogenic and abiogenic phases, are much more complicated than expected previously, and we have little knowledge how well magnetosomes are preserved in bulk sediments. To establish effective criteria for identification of magnetofossils in sediment sample, rock magnetic studies in combination of electron microscopy analyses and ferromagnetic resonance (FMR) spectroscopy are required. Kopp & Kirschvink (2008) recently proposed six-criteria scoring schemes for evaluating identifications, and stressed the FMR spectroscopy as a tool for investigating both the narrowness of grain size distributions and magnetic anisotropy. With these new comprehensive approaches, it is expected that future studies of sediments and sedimentary rocks will unravel more palaeoenvironmental and magnetic signals carried by magnetofossils.

5 CONCLUSIONS

The combination of multiparameter rock magnetic analyses and TEM observations consistently featured the processes of the magnetosome formation in AMB-1 under a controlled microaerobic growth condition. It was found that AMB-1 form magnetite magnetosomes during both the exponential and stationary growth phases, but dominantly in the former one. The growing magnetosomes are organized into 3–5 subchains, linearly aligned along the long axis of the cell. Together with the constant d_{cc} values, observations of this study provide lines of evidence that magnetosomes are physically connected to the cell and linearly assembled. The subchains behave as uniaxial SD particles with strong intra-subchain magnetostatic interactions and rather weak inter-subchain and intercell magnetostatic interactions as shown by highly suppressed vertical distributions in FORC diagrams. The Moskowitz test was proven to be valid for magnetosome arranged in subchains.

ACKNOWLEDGMENTS

We are grateful to the instructive comments from C.L. Deng, D. Schüler, and M.J. Dekkers on an earlier manuscript. We thank C.G. Langereis, M. Winklhofer and anonymous for their useful review to improve the manuscript. We also thank R.J. Harrison and H.F. Qin for discussions on the FORC diagrams. This work was supported by the Chinese Academy of Sciences (grant KZCX-3-sw-150), the National Natural Science Foundation of China (grants 40325011 and 40821091) and the Natural Science Fund of Shandong Province, China (grant 2006ZRB01973). Y.X. Pan and Q.S. Liu were supported by the '100 Talent Program of the Chinese Academy of Sciences'.

REFERENCES

Aragón, R., Gehring, P.M. & Shapiro, S.M., 1993. Stoichiometry, percolation, and Verwey ordering in magnetite, *Phys. Rev. Lett.,* **70,** 1635–1638.

Arató, B., Szanyi, Z., Flies, C., Schüler, D., Frankel, R.B., Buseck, P.R. & Pósfai, M., 2005. Crystal-size and shape distributions of magnetite from uncultured magnetotactic bacteria as a potential biomarker, *Am. Mineral.,* **90,** 1233–1240.

Bazylinski, D.A. & Frankel, R.B., 2004. Magnetosome formation in prokaryotes, *Nat. Rev. Microbiol.,* **2,** 217–230.

Carter-Stiglitz, B., Moskowitz, B.M. & Jackson, M., 2001. Unmixing magnetic assemblages and the magnetic behavior of bimodal mixtures, *J. geophys. Res.,* **106,** 26 397–26 412.

Carter-Stiglitz, B., Moskowitz, B.M. & Jackson, M., 2004. More on the low-temperature magnetism of stable single domain magnetite: reversibility and non-stoichiometry, *Geophys. Res. Lett.,* **31,** L06606, doi:10.1029/02003GL019155.

Chang, S.-B.R., Stolz, J.F., Kirschvink, J.L. & Awramik, S.M., 1989. Biogenic magnetite in stromatolites. II. Occurrence in ancient sedimentray environments, *Precambrian Res.,* **43,** 305–315.

Chen, A.P., Egli, R. & Moskowitz, B.M., 2007. First-order reversal curve (FORC) diagrams of natural and cultured biogenic magnetic particles, *J. geophys. Res.,* **112,** B08S90, doi:10.1029/2006JB004575.

Devouard, B., Pósfai, M., Hua, X., Bazylinski, D.A., Frankel, R.B. & Buseck, P.R., 1998. Magnetite from magnetotactic bacteria: size distributions and twinning, *Am. Mineral.,* **83,** 1387–1398.

Dunin-Borkowski, R.E., McCartney, M.R., Frankel, R.B., Bazylinski, D.A., Pósfai, M. & Buseck, P.R., 1998. Magnetic microstructure of magnetotactic bacteria by electron holography, *Science,* **282,** 1868–1870.

Dunlop, D.J., 2002. Theory and application of the Day plot (M_{rs}/M_s versus H_{cr}/H_c) 1. Theoretical curves and tests using titanomagnetite data, *J. geophys. Res.,* **107,** 2056, doi:10.1029/2001JB000486.

Eberl, D.D., Drits, V.A. & Srodon, J., 1998. Deducing growth mechanisms for minerals from the shapes of crystal size distributions, *Am. J. Sci.,* **298,** 499–533.

Egli, R., 2004. Characterization of individual rock magnetic components by analysis of remanence curves. 3. Bacterial magnetite and natural processes in lakes, *Phys. Chem. Earth,* **29,** 869–884.

Faivre, D., Böttger, L.H., Matzanke, B.F. & Schüler, D., 2007. Intracellular magnetite biomineralization in bacteria proceeds by a distinct pathway involving membrane-bound ferritin and an iron(II) species, *Angew. Chem. Int. Ed. Engl.,* **46,** 8495–8499.

Fischer, H., Mastrogiacomo, G., Löffler, J.F., Warthmann, R.J., Weidler, P.G. & Gehring, A.U., 2008. Ferromagnetic resonance and magnetic characteristics of intact magnetosome chains in *Magnetospirillum gryphiswaldense, Earth planet. Sci. Lett.,* **270,** 200–208.

Frankel, R.B., Bazylinski, D.A., Johnson, M.S. & Taylor, B.L., 1997. Magneto-aerotaxis in marine coccoid bacteria, *Biophys. J.,* **73,** 994–1000.

Frankel, R.B., Blakemore, R.P. & Wolfe, R.S., 1979. Magnetite in freshwater magnetotactic bacteria, *Science,* **203,** 1355–1356.

Gorby, Y.A., 1989. Regulation of magnetosome biogenesis by oxygen and nitrogen, *PhD thesis*. University of New Hampshire, New Hampshire.

Hanzlik, M., Winklhofer, M. & Petersen, N., 2002. Pulsed-field-remanence measurements on individual magnetotactic bacteria, *J. Magn. Magn. Mater.,* **248,** 258–267.

Hesse, P.P., 1994. Evidence for bacterial paleoecological origin of mineral magnetic cycles in oxic and sub-oxic tasman sea sediments, *Mar. Geol.,* **117,** 1–17.

Housen, B.A. & Moskowitz, B.M., 2006. Depth distribution of magnetofossils in near-surface sediments from the Blake/Bahama Outer Ridge, western North Atlantic Ocean, determined by low-temperature magnetism, *J. geophys. Res.,* **111,** G01005, doi:10.1029/02005JG000068.

Kim, B., Kodama, K. & Moeller, R., 2005. Bacterial magnetite produced in water column dominates lake sediment mineral magnetism: Lake Ely, USA, *Geophys. J. Int.,* **163,** 26–37.

Kobayashi, A., Kirschvink, J.L., Nash, C.Z., Kopp, R.E., Sauer, D.A., Bertani, L.E., Voorhout, W.F. & Taguchi, T., 2006. Experimental observation of magnetosome chain collapse in magnetotactic bacteria: sedimentological, paleomagnetic, and evolutionary implications, *Earth planet. Sci. Lett.,* **245,** 538–550.

Komeili, A., 2007. Molecular mechanisms of magnetosome formation, *Annu. Rev. Biochem.,* **76,** 351–366.

Komeili, A., Li, Z., Newman, D.K. & Jensen, G.J., 2006. Magnetosomes are cell membrane invaginations organized by the actin-like protein MamK, *Science,* **311,** 242–245.

Komeili, A., Vali, H., Beveridge, T.J. & Newman, D.K., 2004. Magnetosome vesicles are present before magnetite formation, and MamA is required for their activation, *Proc. Natl. Acad. Sci. USA,* **101,** 3839–3844.

Kopp, R.E. & Kirschvink, J.L., 2008. The identification and biogeochemical interpretation of fossil magnetotactic bacteria, *Earth Sci. Rev.,* **86,** 42–61.

Kopp, R.E., Nash, C.Z., Kobayashi, A., Weiss, B.P., Bazylinski, D.A. & Kirschvink, J.L., 2006. Ferromagnetic resonance spectroscopy for assessment of magnetic anisotropy and magnetostatic interactions: a case study of mutant magnetotactic bacteria, *J. geophys. Res.,* **111,** B12S25, doi:10.1029/2006JB004529.

Linford, N., Linford, P. & Platzman, E., 2005. Dating environmental change using magnetic bacteria in archaeological soils from the upper Thames Valley, UK, *J. Archaeol. Sci.,* **32,** 1037–1043.

Lippert, P.C. & Zachos, J.C., 2007. A biogenic origin for anomalous fine-grained magnetic material at the Paleocene-Eocene boundary at Wilson Lake, New Jersey, *Paleoceanography,* **22,** PA4104, doi:10.1029/2007PA001471.

Maloof, A.C. *et al*., 2007. Sedimentary iron cycling and the origin and preservation of magnetization in platform carbonate muds, Andros Island, Bahamas, *Earth planet. Sci. Lett.,* **259,** 581–598.

Matsunaga, T., Sakaguchi, T. & Tadokoro, F., 1991. Magnetite formation by a magnetic bacterium capable of growing aerobically, *Appl. Microbiol. Biotechnol.,* **35,** 651–655.

Matsunaga, T., Tsujimura, N. & Kamiya, S., 1996. Enhancement of magnetic particle production by nitrate and succinate fed-batch culture of *Magnetospirillum* sp. AMB-1, *Biotechnol. Tech.,* **10,** 495–500.

Moskowitz, B.M., Bazylinski, D.A., Egli, R., Frankel, R.B. & Edwards, K.J., 2008. Magnetic properties of marine magnetotactic bacteria in a seasonally stratified coastal pond (Salt Pond, MA, USA), *Geophys. J. Int.,* **174,** 75–92.

Moskowitz, B.M., Frankel, R.B. & Bazylinski, D.A., 1993. Rock magnetic criteria for the detection of biogenic magnetite, *Earth planet. Sci. Lett.,* **120,** 283–300.

Muxworthy, A., Heslop, D. & Williams, W., 2004. Influence of magnetostatic interactions on first-order-reversal-curve (FORC) diagrams: a micromagnetic approach, *Geophys. J. Int.,* **158,** 888–897.

Muxworthy, A.R. & McClelland, E., 2000. Review of the low-temperature magnetic properties of magnetite from a rock magnetic perspective, *Geophys. J. Int.,* **140,** 101–114.

Newell, A.J., 2005. A high-precision model of first-order reversal curve (FORC) functions for single-domain ferromagnets with uniaxial anisotropy, *Geochem. Geophys. Geosyst.,* **6,** Q05010, doi:10.1029/02004GC000877.

Pósfai, M., Kasama, T. & Dunin-Borkowski, R.E., 2006a. Characterization of bacterial magnetic nanostructures using high-resolution transmission electron microscopy and off-axis electron holography, in *Magnetoreception and Magnetosomes in Bacteria,* pp. 197–225, ed. Schüler, D., Springer-Verlag, Berlin.

Pósfai, M., Moskowitz, B.M., Arató, B., Schüler, D., Flies, C., Bazylinski, D.A. & Frankel, R.B., 2006b. Properties of intracellular magnetite crystals produced by *Desulfovibrio magneticus* strain RS-1, *Earth planet. Sci. Lett.,* **249,** 444–455.

Paasche, O., Lovlie, R., Dahl, S., Bakke, J. & Nesje, A., 2004. Bacterial magnetite in lake sediments: late glacial to Holocene climate and sedimentary changes in northern Norway, *Earth planet. Sci. Lett.,* **223,** 319–333.

Pan, Y.X., Petersen, N., Davila, A.F., Zhang, L.M., Winklhofer, M., Liu, Q.S., Hanzlik, M. & Zhu, R.X., 2005a. The detection of bacterial magnetite in recent sediments of Lake Chiemsee (southern Germany), *Earth planet. Sci. Lett.,* **232,** 109–123.

Pan, Y.X., Petersen, N., Winklhofer, M., Davila, A.F., Liu, Q.S., Frederichs, T., Hanzlik, M. & Zhu, R.X., 2005b. Rock magnetic properties of uncultured magnetotactic bacteria, *Earth planet. Sci. Lett.,* **237,** 311–325.

Penninga, I., Dewaard, H., Moskowitz, B.M., Bazylinski, D.A. & Frankel, R.B., 1995. Remanence measurements on individual magnetotactic bacteria using a pulsed magnetic-field, *J. Magn. Magn. Mater.,* **149,** 279–286.

Pike, C.R., Roberts, A.P. & Verosub, K.L., 1999. Characterizing interactions in fine magnetic particle systems using first order reversal curves, *J. Appl. Phys.,* **85,** 6660–6667.

Prozorov, R., Prozorov, T., Williams, T.J., Bazylinski, D.A., Mallapragada, S.K. & Narasimhan, B., 2007. Magnetic irreversibility and Verwey transition in nano-crystalline bacterial magnetite, *Phys. Rev. B,* **76,** 054406, doi:10.1103/physRevB054476.054406.

Roberts, A.P., Pike, C.R. & Verosub, K.L., 2000. First-order reversal curve diagrams: a new tool for characterizing the magnetic properties of natural samples, *J. geophys. Res.,* **105,** 28 461–28 476.

Scheffel, A., Gruska, M., Faivre, D., Linaroudis, A., Plitzko, J.M. & Schüler, D., 2006. An acidic protein aligns magnetosomes along a filamentous structure in magnetotactic bacteria, *Nature,* **440,** 110–114.

Simmons, S.L. & Edwards, K.J., 2006. Geobiology of magnetotactic bacteria, in *Magnetoreception and magnetosomes in bacteria,* pp. 77–102, ed. Schüler, D., Springer-Verlag, Berlin.

Simmons, S.L., Sievert, S.M., Frankel, R.B., Bazylinski, D.A. & Edwards, K.J., 2004. Spatiotemporal distribution of marine magnetotactic bacteria in a seasonally stratified coastal salt pond, *Appl. Environ. Microbiol.,* **70,** 6230–6239.

Simpson, E.T., Kasama, T., Pósfai, M., Buseck, P.R., Harrison, R.J. & Dunin-Borkowski, R.E., 2005. Magnetic induction mapping of magnetite chains in magnetotactic bacteria at room temperature and close to the Verwey transition using electron holography, *J. Phys.: Conf. Ser.,* **17,** 108–121.

Snowball, I., Zillen, L. & Sandgren, P., 2002. Bacterial magnetite in Swedish varved lake-sediments: a potential bio-marker of environmental change, *Quat. Int.,* **88,** 13–19.

Stoner, E.C. & Wohlfarth, E.P., 1948. A mechanism of magnetic hysteresis in heterogeneous alloys, *Phil. Trans. R. Soc. Lond. Ser. A.,* **240,** 599–642.

Walz, F., 2002. The Verwey transition—a topical review, *J. Phys.,* **14,** R285–R340.

Weiss, B.P., Kim, S.S., Kirschvink, J.L., Kopp, R.E., Sankaran, M., Kobayashi, A. & Komeili, A., 2004. Ferromagnetic resonance and low-temperature magnetic tests for biogenic magnetite, *Earth planet. Sci. Lett.,* **224,** 73–89.

Winklhofer, M., Dumas, R.K. & Liu, K., 2008. Identifying reversible and irreversible magnetization changes in prototype patterned media using first- and second-order reversal curves, *J. Appl. Phys.,* **103,** 07C518, doi:10.1063/1061.2837888.

Winklhofer, M. & Zimanyi, G.T., 2006. Extracting the intrinsic switching field distribution in perpendicular media: a comparative analysis, *J. Appl. Phys.,* **99,** 08E710, doi:10.1063/1061.2176598.

Yang, C.D., Takeyama, H., Tanaka, T. & Matsunaga, T., 2001. Effects of growth medium composition, iron sources and atmospheric oxygen concentrations on production of luciferase-bacterial magnetic particle complex by a recombinant *Magnetospirillum magneticum* AMB-1, *Enzyme Microb. Technol.,* **29,** 13–19.

APPENDIX

A.1 Chemical composition of growth medium

The modified MSGM used in this study contains the following ingredients (in grams per litre): 0.74 g of succinic acid, 0.68 g of potassium dihydrogen phosphate, 0.12 g of sodium nitrate and 0.1 g of sodium thioglycolate. The medium was supplemented with 10 mL of Wolfe's vitamin solution and 10 mL of Wolfe's mineral solution. The pH was adjusted to 7.0 with NaOH solution prior to sterilization at 115 °C for 30 min. Compared with the normal MSGM, our modified MSGM contains three-fold more ferric quinate (60 μM) and is enriched by the addition of 0.1 g yeast extract and 0.2 g of polypeptone. The addition of yeast extract and polypeptone was proven to be able to increase the cell growth and magnetosome production (Yang *et al*. 2001).

A.2 Preparation and inoculation of non-magnetic AMB-1 cells

First, the pre-cultured cells were inoculated into 200 mL MSGM contained in a 300-mL flask. The initial cell density is about 2.0×10^6cells mL^{-1} (measured by bacterial counting chamber). The flask was then put in a shaking incubator with free gas exchange and was agitated at 80 rpm at 26 °C. After 36 hr shaking cultivation, the cells reached an exponential growth phase with cell density of about 5.0×10^8 cells mL^{-1}. The newly divided cells did not contain intracellular magnetic particles based on TEM observations. The non-magnetic AMB-1 cells were obtained through a 36-hr aerobic incubation of AMB-1 strains. About 2-mL non-magnetic AMB-1 cell suspension was inoculated into each of the 96 250-mL serum vials (the initial density of cells is approximately 2.0×10^6 cells mL^{-1}). To generate a microaerobic condition, the vials were sealed with butyl-rubber stopper after the inoculation to avoid further gas exchange with ambient air.